Carbohydrate Polymers 95 (2013) 348–359

Contents lists available at SciVerse ScienceDirect

Carbohydrate Polymers

journal homepage: www.elsevier.com/locate/carbpol

Preparation and characterization of some graphene based nanocomposite materials

Shabnam Sheshmani*, Raheleh Amini

Department of Chemistry, Shahr-e-Rey Branch, Islamic Azad University, P.O. Box 18155-144, Tehran, Iran

ARTICLE INFO

Article history:
Received 24 December 2012
Received in revised form 27 February 2013
Accepted 3 March 2013
Available online 13 March 2013

Keywords:
Graphene
Graphene oxide
Nanocomposite
Matrix

ABSTRACT

In this study, graphene based sheets such as graphene oxide (GO) and graphene (G) were produced via a facile preparation route involving graphite oxidation, ultrasonic exfoliation and chemical reduction. Also, this paper reports simple approaches for deposition of manganese dioxide, ferric hydroxide and cobalt nanoparticles onto the surface of the graphene based sheets. Chemical deposition method of metal salt with graphene based sheets was performed to prepare nanocomposites. The structural, surface and characteristics of the GO, G and their nanocomposites were investigated by Fourier transform infrared spectroscopy, Raman spectroscopy, powder X-ray diffraction, scanning electron microscopy, energy dispersive X-ray spectroscopy, atomic force microscopy and X-ray photoelectron spectroscopy. The results demonstrated that interaction between GO as matrix and metal nanoparticles were via hydroxyl, carbonyl and/or carboxylate groups. The metal nanoparticles were homogeneously distributed on the matrix of composite.

© 2013 Elsevier Ltd. All rights reserved.

1. Introduction

Graphene based sheets (GBS) such as graphene oxide (GO) and graphene (G) have stimulated great interest due to their promising electronic, mechanical, and thermal properties (Berger et al., 2004, 2006; Hirata, Gotou, Horiuchi, Fujiwara, & Ohba, 2004; Metin, Kayhan, Özkar, & Schneider, 2012; Novoselov et al., 2004, 2005; Siamaki, Khder, Abdelsayed, El-Shall, & Gupton, 2011; Truong-Huu et al., 2012; Zhang, Small, Amori, & Kim, 2005; Zhang, Tan, Stormer, & Kim, 2005).

Graphene is two-dimensional nanomaterial consisting of a single layer of sp^2 network of carbon atoms. While the thickness of a graphene sheet is on the order of a single atomic unit, its lateral dimension can approach up to tens of microns (Novoselov et al., 2004). Initially, graphene was prepared at the individual sheet level by mechanical exfoliation from highly ordered pyrolytic graphite (HOPG) crystals the so-called Scotch tape trick (Novoselov et al., 2004). To scale up the production, various synthetic methods were developed. At a slightly larger scale, high quality graphene thin films have been prepared epitaxial on SiC surface (Berger et al., 2004) and most recently by chemical vapor deposition (CVD) on catalytic metal surfaces (Reina et al., 2009). At an even larger scale, bulk production typically yields GBS in forms of solvent dispersion, which can then be used by solution processing techniques. Some recent success includes chemical exfoliation, solvent assisted ultrasonic exfoliation and solvothermal reduction (Dikin et al., 2007; Stankovich et al., 2006; Wang et al., 2008).

One possible technique of preventing aggregation and harnessing the unique properties of single-layer graphene would be to incorporate graphene sheets into composite materials. Many metal or metal oxide nanoparticles, such as Au, Ag, Pt, Pd, TiO_2 and SnO_2 have been deposited on graphene sheets. These metal or metal oxide nanoparticles not only prevent the aggregation of graphene sheets into graphite but also combine with the special two-dimensional graphene, giving rise to some unique electronic, optical and catalytical properties which may be used in applications, such as biologic sensing, photocatalysis, optoelectronic and electrochemical devices (Guo et al., 2011; Singh et al., 2009; Subrahmanyam, Manna, Pati, & Rao, 2010; Wang et al., 2010). The manufacturing of such composites requires not only the graphene sheets which be produced on a sufficient scale but that they also be incorporated and homogeneously distributed into various matrices.

This work reports a general approach for the preparation of graphene oxide and graphene sheets. Deposition of manganese dioxide, ferric hydroxide and cobalt nanoparticles onto surfaces of graphene were also investigated by chemical deposition method. The structure of the chemically graphene oxide, graphene and synthesized composites were characterized using Fourier

* Corresponding author. Tel.: +98 21 5522 9200; fax: +98 21 5522 9297.
E-mail address: shabnam_sheshmani@yahoo.com (S. Sheshmani).

0144-8617/$ – see front matter © 2013 Elsevier Ltd. All rights reserved.
http://dx.doi.org/10.1016/j.carbpol.2013.03.008

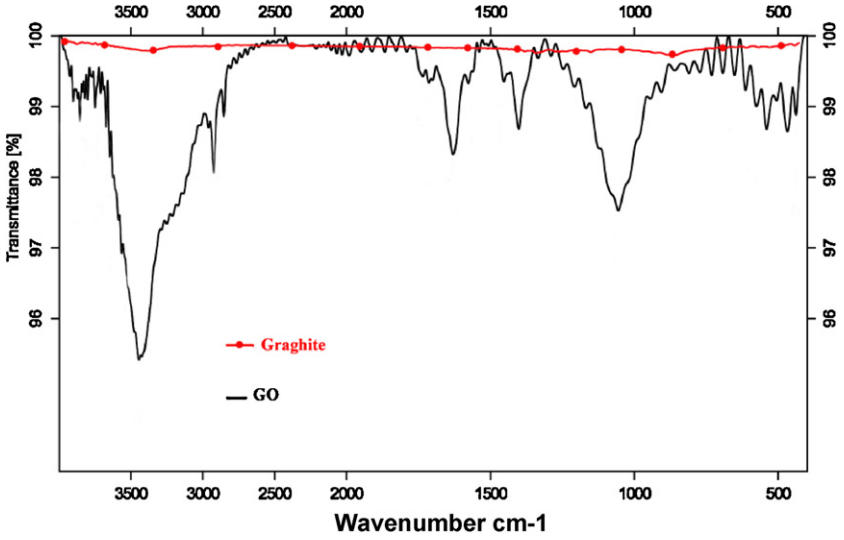

Fig. 1. FT-IR spectra of graphite and graphite oxide. (For interpretation of the references to color in this figure legend, the reader is referred to the web version of this article.)

transform infrared spectroscopy, Raman spectroscopy, powder X-ray diffraction, scanning electron microscopy, energy dispersive X-ray spectroscopy, atomic force microscopy and X-ray photoelectron spectroscopy.

2. Experimental

2.1. Materials

Graphite flakes was purchased from Sigma–Aldrich with a particle size of 150 μm and purity of 99.9%. All of the other solvents and materials were of analytical grade, commercially available and used without further purification.

2.2. Synthesis of graphite oxide

Graphite oxide was prepared according to the Staudenmaier method (Staudenmaier, 1898) as follow. A reaction flask containing a magnetic stir bar was charged with nitric acid (9 mL) and sulfuric acid (18 mL) and cooled by immersion in an ice bath. The acid mixture was stirred and allowed to cool for 15 min and graphite (1 g) was added under vigorous stirring to avoid agglomeration. After the

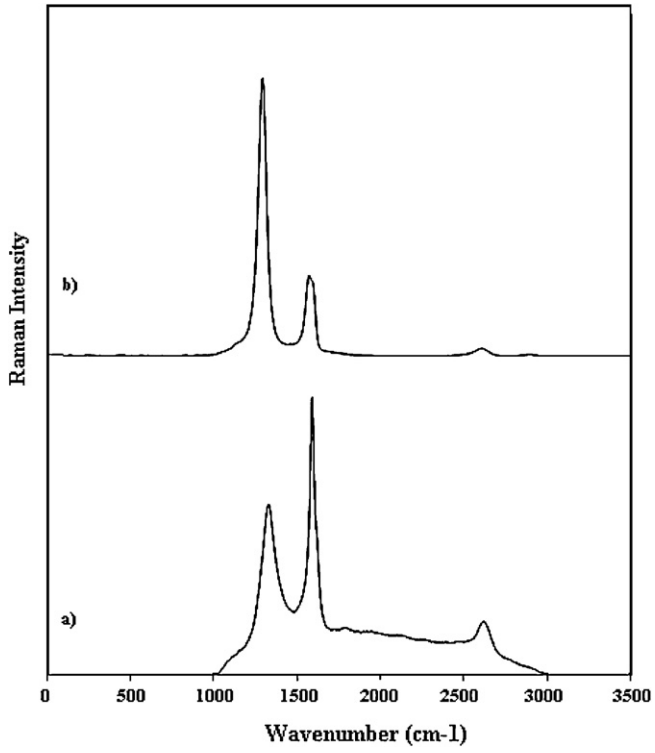

Fig. 2. Raman spectra of (a) graphite oxide and (b) graphene.

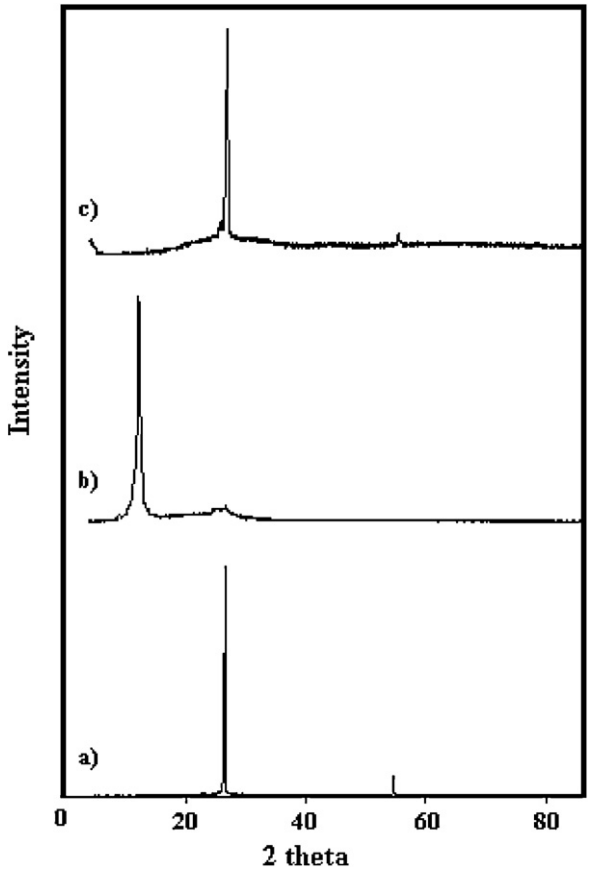

Fig. 3. X-ray diffraction patterns of (a) graphite (b) graphite oxide and (c) graphene.

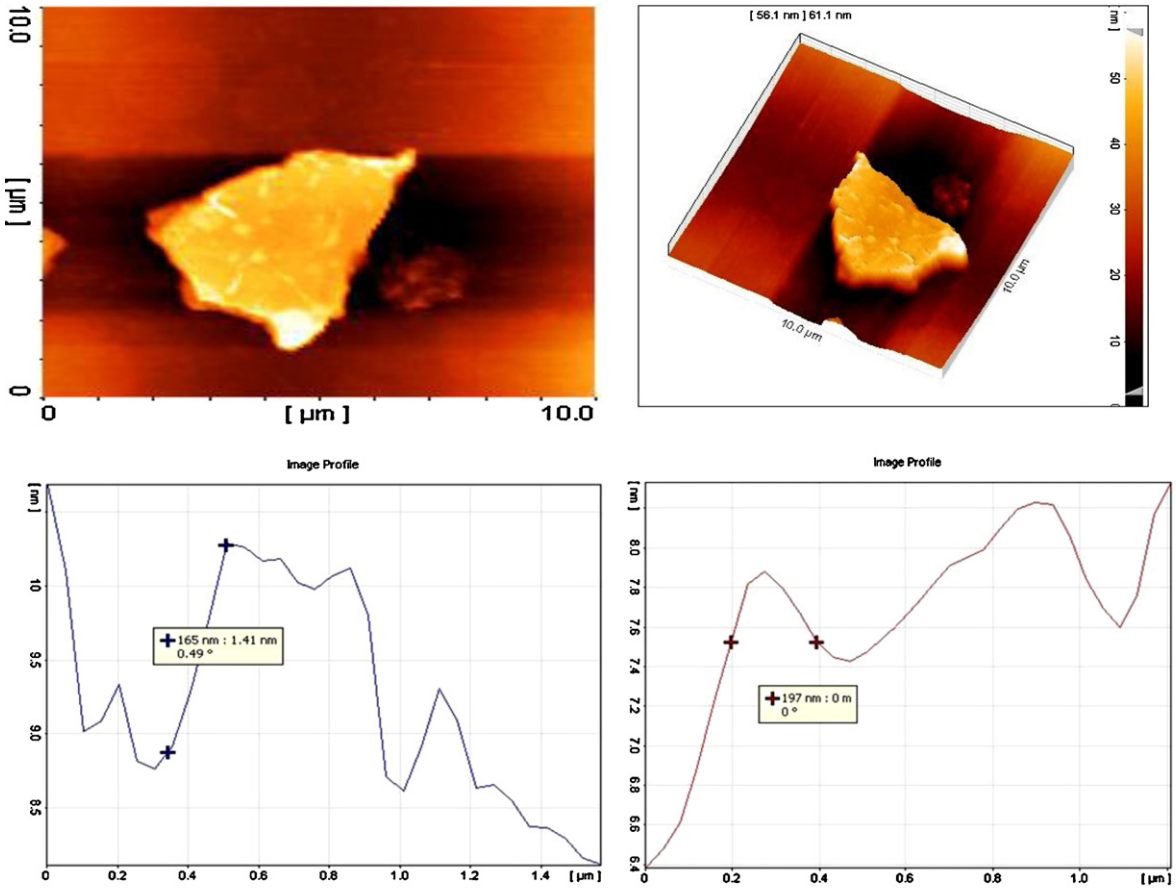

Fig. 4. AFM images of exfoliated graphene oxide sheets.

graphite powder was well dispersed, potassium chlorate (11 g) was added slowly over 2 h to avoid sudden increases in temperature and allowed to stir for 96 h at room temperature. On completion of the reaction, the mixture was poured into deionized water (100 mL) and filtered. The graphite oxide was re-dispersed and washed in a 5% solution of hydrochloric acid. Then, the product was washed repeatedly with deionized water until the pH of the filtrate was neutral and finally vacuum dried.

2.3. Synthesis of graphene nanosheets

For the preparation of graphene nanosheets using sodium borohydride ($NaBH_4$) (0.2 g) as reducing agent, graphite oxide (0.1 g) was dispersed in water (20 mL) through ultrasonication. The mixture was allowed to stir for 30 min and then heated at 100 °C for 3 h. The black solid was isolated by centrifugation, washed with water and acetone and finally oven-dried.

2.4. Synthesis of MnO_2/G nanocomposite

In order to prepare MnO_2/G nanocomposite, synthesized graphene powder (0.10 g) was dispersed in water (50 mL) with the aid of ultrasonication vibration for 30 min. Following the procedure, to this suspension, $KMnO_4$ (0.05 g) was added. The mixture was stirred for 30 min and heated for 15 min. Finally, the black solid was filtered and washed with distilled water and ethanol, dried at 90 °C for 10 h in a vacuum oven.

2.5. Synthesis of $Fe(OH)_3$/GO nanocomposite

For the synthesis of $Fe(OH)_3$/GO nanocomposite, graphite oxide (0.30 g) was dispersed into water (20 mL) by ultrasonication vibration for 45 min. Consequently, $Fe(NO_3)_2{\cdot}9H_2O$ (0.12 g) was added. The mixture was stirred for 12 h at room temperature. To this suspension, H_2O_2 (1 mL) was added during approximately 1 h. After 24 h, ammonium hydroxide was added until the pH reached 8. The water in the reaction mixture was evaporated. The black solid was washed with warm water and dried in a vacuum oven at 85 °C for overnight.

2.6. Synthesis of Co/G nanocomposite

Cobalt/G nanocomposite was prepared from the reaction between synthesized graphite oxide (0.30 g) in ethylene glycol (50 mL) with $Co(NO_3)_2{\cdot}6H_2O$ (0.10 g) in ethylene glycol (30 mL). Subsequently, sodium borohydride (1.5 mL) was added into the mixed solution. After ultrasonication for 30 min, this mixture was refluxed for 5 h. The resultant solid products were separated by centrifugation, washed with distilled water and ethanol, and finally dried at 50 °C for 24 h in a vacuum oven.

2.7. Characterizations

Infrared spectra were recorded as KBr disks on Tensor 27 Bruker spectrophotometer. Raman spectroscopy investigated using a Senterra Bruker with 785 nm diode laser excitation. The evaluation of synthesized graphene oxide, graphene and nanocomposites

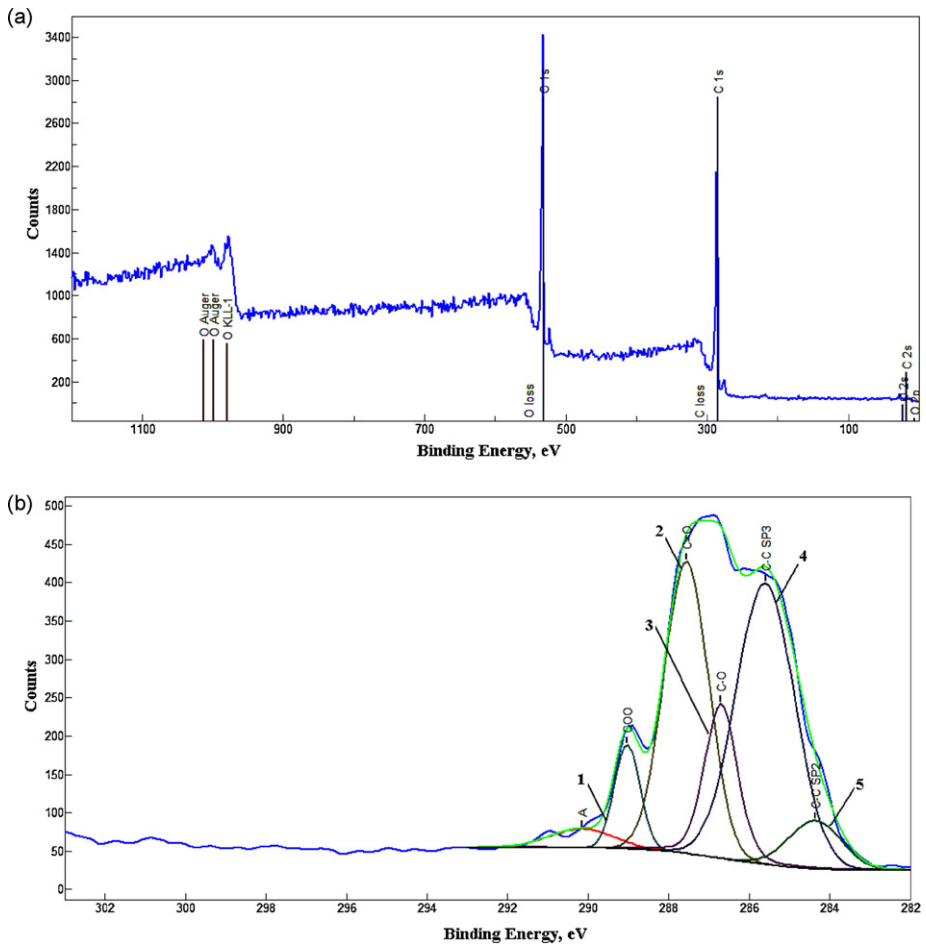

Fig. 5. XPS (a) general and (b) curve fit of C1s spectra of graphite oxide.

during the processes was monitored by powder X-ray diffraction Philips PW 1800 diffractometer with Cu Kα radiation. Scanning electron microscopy measurements and Energy Dispersive X-ray spectroscopy were performed on a MIRA\\TESCAN at an accelerating voltage of 20 kV. Atomic force microscopy was carried out on a Denmark Dualscope/Rasterscope C26, DME microscope. The surface chemistries of graphene oxide and $Fe(OH)_3$/GO nanocomposite were characterized on X-ray photoelectron spectroscope (XPS, surface analysis EA10 plus). The XPS was equipped with Al–Mg anode. The vacuum-dried samples was employed to detect the element compositions. To identify the types and percentages of the functional groups on the surface of the above samples, the C 1s, O 1s and Fe 2p peaks of the XPS spectra were curve-fitted.

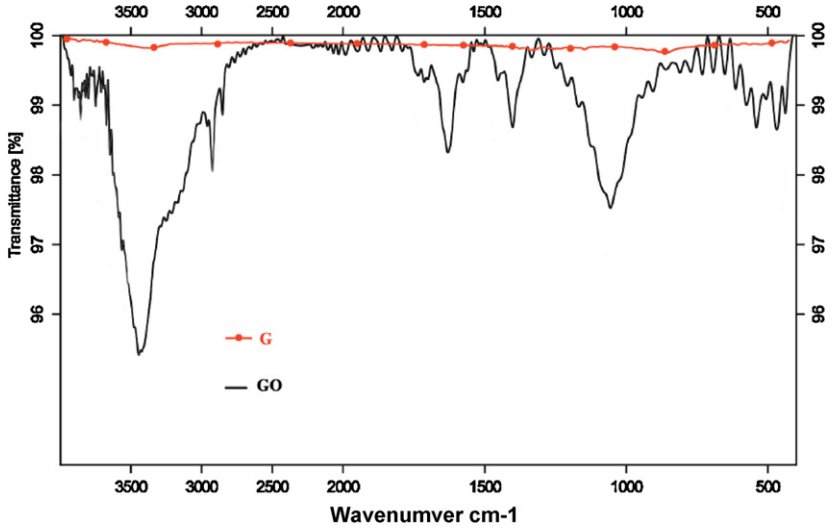

Fig. 6. FT-IR spectra of graphite oxide and graphene. (For interpretation of the references to color in this figure legend, the reader is referred to the web version of this article.)

3. Results and discussion

Recently, graphene as carbonaceous matrix, for preparation of composites have been investigated. Therefore, the suitable preparation is important for the industrialization of its applications. To date, monolayer or few-layer graphene has been prepared by some different methods, including micromechanical cleavage, chemical vapor deposition and epitaxial growth methods. However, some of these need harsh reaction conditions and some have tedious step, which are unable to meet the requirements of industrial production. It should be emphasized that, currently, only the chemical exfoliation method is considered as a common route toward the production of graphene at low cost and in a large quantity. It first involves the oxidation of well-stacked graphite to graphite oxide and is then followed by chemical reduction to obtain reduced graphene oxide (RGO) or thermal exfoliation of graphite oxide to produce graphene. Generally, oxidation results in an increase of the *d*-spacing and intercalation between adjacent graphene layers and thus weakens the interaction between adjacent sheets and finally leads to the dispersion of graphite oxide in an aqueous solution. Reduction using chemical compounds such as hydroquinone, hydrazine hydrate, potassium hydroxide, sodium borohydride or thermal exfoliation of graphite oxide is commonly performed to obtain graphene from graphite oxide.

There have been a few reports on the deposition of particles such as manganese dioxide, ferric hydroxide and cobalt on graphene oxide or graphene synthesized by modified hummers method (Ji, Shena, Song, & Zhu, 2011; Yan et al., 2010; Zhang, Dwivedi, Chi, & Wu, 2010), while in this study, employed graphene oxide was prepared through Staudenmaier method as a facile procedure.

3.1. Characterization of graphite oxide

The FT-IR spectra of graphite and graphite oxide are shown in Fig. 1. Comparison of these spectra clearly shows the characteristic peaks of graphene oxide such as the stretching vibration of hydroxyl group (—OH), the stretching vibration of C=O from carboxylic group, the vibration of O=C—O from carboxylate, the vibration of C—O alcohol and C—O—C of epoxy groups centered at 3443, 1735, 1401, 1207 and 1055 cm^{-1}, respectively. Also, the peak at 1629 cm^{-1} is attributed to the vibrations of the adsorbed water molecules and also the vibrations of unoxidized graphitic domains, in the sample. The presence of various oxygen bearing functional groups (C=O, C—O, —OH) in the structure of graphene oxide, can lead to synthesis of various composites with varied properties.

Raman spectroscopy is a powerful nondestructive tool to characterize carbon materials, particularly for distinguishing ordered and disordered crystal structures of carbon. The oxidation leads to a huge reduction in the size of graphite nanosheets in graphite oxide, compared to the size of the natural graphite flakes. The Raman spectrum of the graphite oxide displays a strong G line at 1592 cm^{-1} assigned to the E_{2g} phonon of carbon sp^2 atoms, while the D line at 1332 cm^{-1} attributed to a breathing mode of phonons of A_{1g} symmetry, which is attributed to local defects and disorders. The overtone of the D line is located at 2622 cm^{-1} (Fig. 2a).

The oxidation results showed an increase in the interlayer spacing of graphite nanosheets in graphite oxide relative to natural graphite, which can be attributed to the intercalation of oxygen-based groups or ions between its layers. Hence, the interlayer distance of graphite can be increased from 3.35 Å of the original graphite to 6–10 Å, depending on water content and the extent of the intercalation process (Hontoria-Lucas, López-Peinado, López-González, & Martin-Aranda, 1995). As mentioned earlier, a mixture of nitric acid, sulfuric acid and potassium chlorate was used to oxidize the natural graphite powders. During this process, epoxy and hydroxyl groups lie on the surface of each graphene layer, while the carboxyl groups are located near the edges of basal planes of the graphite structure. Simultaneously, carbon hydrolyzation occurred and the sp^2 bonds changed to sp^3 bonds. At the same time, H_2O, NO_3^-, or SO_4^{2-} ions could insert themselves into the graphene layer, inducing an increase in the interlayer spacing (He, Klinowski, Foster, & Lerf, 1998; Hontoria-Lucas et al., 1995). The graphite oxidation process was monitored using powder X-ray diffraction. Fig. 3a and b shows the XRD pattern of the graphite and graphite oxide after oxidation for 4 days. As oxidation proceeds, the intensity of the (0 0 2) diffraction line *d*-space 3.35 Å at 26.4° in natural graphite gradually weakened and finally disappeared. Simultaneously, the graphite oxide exhibited only one peak at 12.2°. The interlayer distance between neighboring graphene layers in graphite oxide has increased with oxidation (they are

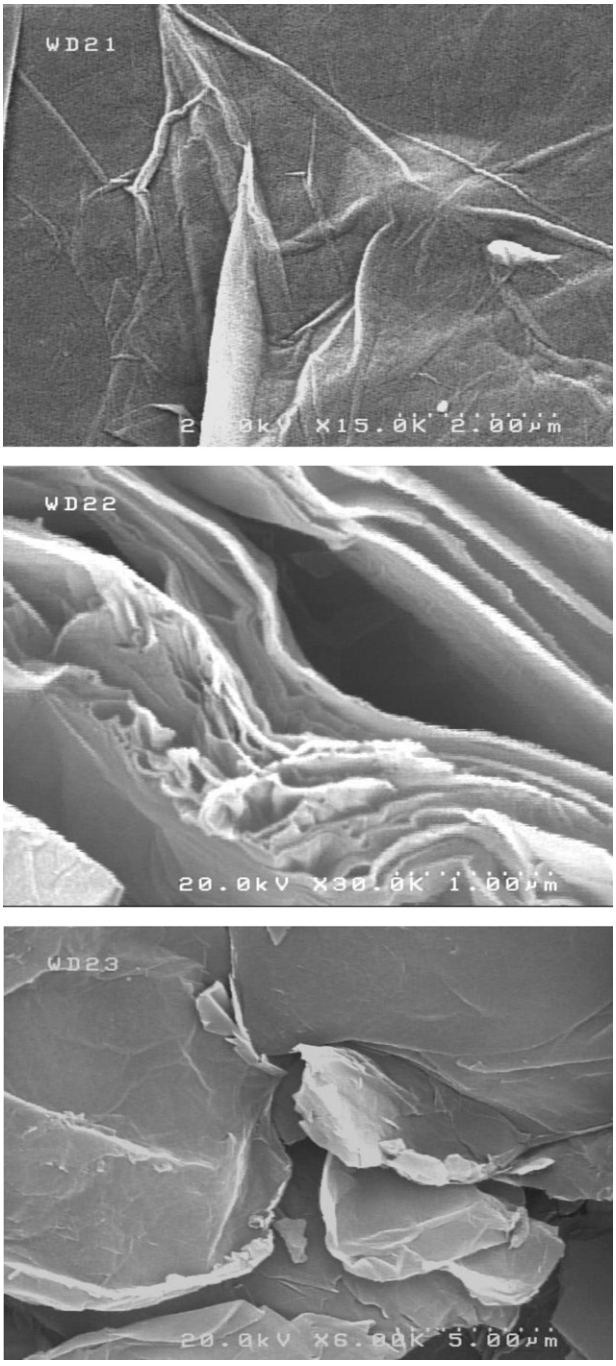

Fig. 7. SEM micrographs of graphene nanosheets.

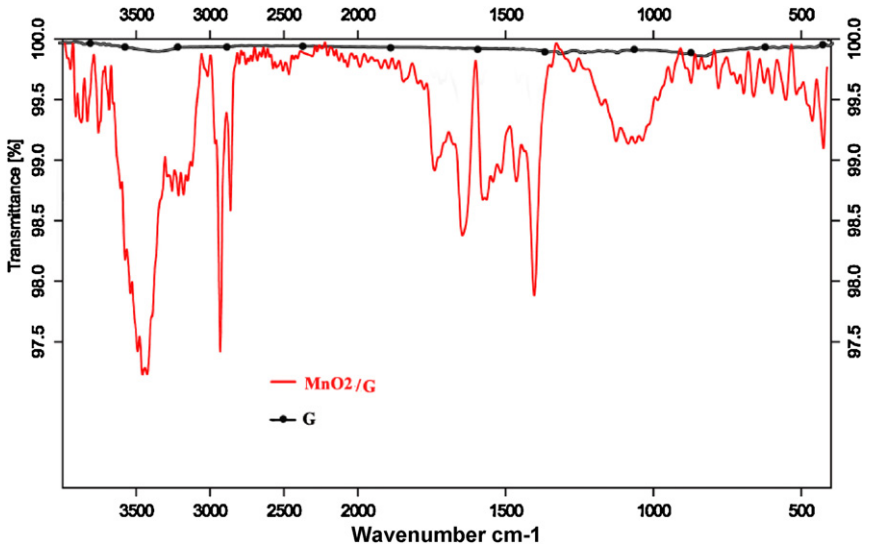

Fig. 8. FT-IR spectra of graphene and MnO_2/G. (For interpretation of the references to color in this figure legend, the reader is referred to the web version of this article.)

~7.22 Å apart), because of the intercalation by oxygen-containing groups and moisture. In 4-day of chemical treatment, the graphite powders were completely oxidized to graphite oxide. Increasing the reaction time (>96 h) did not show any remarkable effect on the oxidation reaction (proved by the absence of further changes in the XRD analysis).

The exfoliation to achieve graphene oxide plates has been most typically confirmed by thickness measurements of the single graphene sheet (~1.1 nm height) using atomic force microscopy (AFM) (Fig. 4).

The surface information of graphene oxide was collected by XPS. To identify the functional groups and the respective percentages, both the general XPS spectra and the curve-fitted C 1s spectra are presented in Fig. 5. The functionalities numbered from 1 to 5 are specified in Table 1. XPS further illustrates the present of cabon–oxygen bonds. This phenomenon was mainly attributed to the generation of oxygenated functional groups, such as epoxide, hydroxyl, carbonyl and carboxyl groups, which broke the carbon sigma bonds and transformed them into single C—C or sp^3 bonds. The peaks of O 1s and C 1s can be observed in the survey spectrum. These functional groups were further confirmed by the FT-IR spectroscopy.

3.2. Characterization of graphene

The FT-IR spectrum of graphene obtained from sodium borohydride as reducing agent is illustrated in Fig. 6. Interestingly, considerable changes are also observed in the IR spectra of graphene oxide before and after treatment with sodium borohydride, and giving evidence for the eliminated all vibration bands attributed to oxygen-containing groups after the reduction and thus the graphene oxide was effectively transformed into graphene in the syntheses.

Raman spectroscopy was employed to analyze the structural changes during chemical processing from graphite oxide to reduced graphite oxide. After chemical reduction of graphene oxide, the conjugated graphene network (sp^2 carbon) will be reestablished. However, the size of the reestablished graphene network is

Table 1
Functional groups obtained from curve fitting of C 1s XPS spectra (%) in graphene oxide.

	BE (eV)	FWHM (eV)	Peak area (cts)	Rel (%)
1: COO	289.03	0.75	108.2	6.4
2: C=O	287.56	1.30	528.8	31.4
3: C—O	286.70	0.96	225.1	13.4
4: C—C SP^3	285.60	1.71	668.0	39.7
5: C—C SP^2	284.36	1.53	103.0	6.1

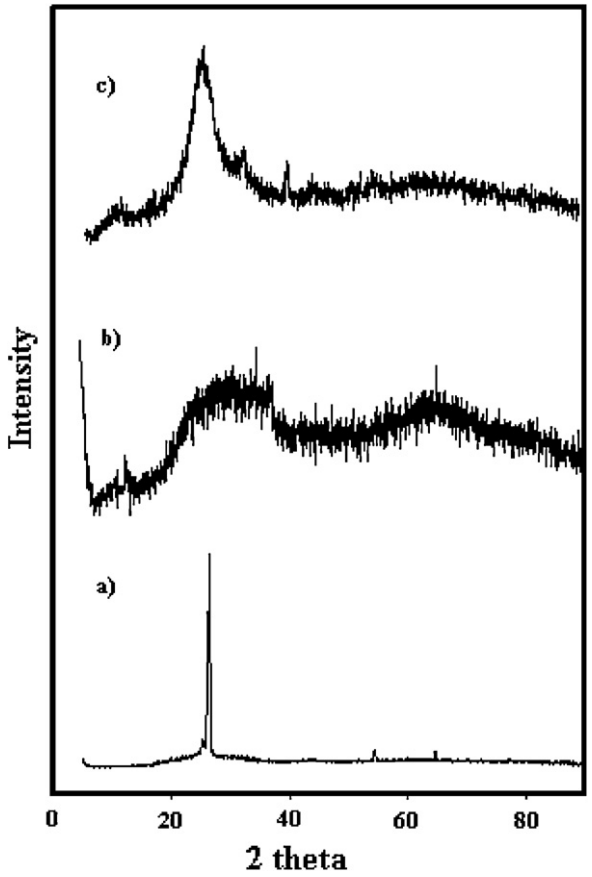

Fig. 9. XRD patterns of (a) MnO_2/G, (b) $Fe(OH)_3$/GO and (c) Co/G nanocomposites.

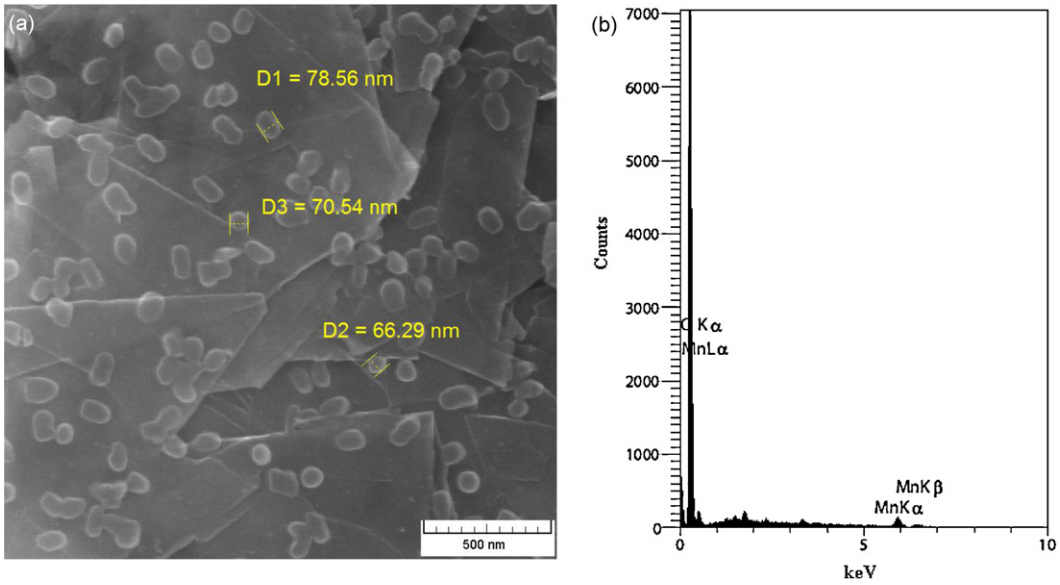

Fig. 10. (a) SEM micrographs and (b) corresponding EDS patterns of MnO_2/G nanocomposite.

usually smaller than the original graphite layer, which will lead to the increase of intensity of the D/G consequently. As it can be seen from Fig. 2b, the Raman spectrum of RGO contains both G and D bands which shifted back to 1584 and 1312 cm^{-1}, respectively.

Fig. 3c shows the XRD pattern of graphene after treatment with sodium borohydride. The interlayer distance obtained from graphene oxide is 7.22 Å ($2\theta = 12.2^\circ$) with reduction, the interlayer distance is expected to contract due to the removal of such functional groups. The peak of the large interlayer distance disappeared completely and a peak near 3.356–3.361 Å ($2\theta = 26.5^\circ$) became visible. This implied that most of the functional groups were removed, and it should be noted that XRD pattern were similar to that of graphite (Fig. 3a).

The microstructure images of graphene are shown in Fig. 7. Graphene from reduction of graphene oxide have wrinkles and folds of edges and exhibit a typically sheet-like structure (57 nm in thickness).

3.3. Characterization of MnO_2/G nanocomposite

MnO_2/G nanocomposites were prepared by redox reaction. In this reaction, graphene substrate serves as a reductant and converts aqueous permanganate (MnO_4^-) to insoluble MnO_2, which deposits on the surfaces of graphene. Result of redox reaction is formation of MnO_2, CO_3^{2-} and HCO_3^- (Yan et al., 2010). Then, many oxygen-containing functionalities such as —OH, C=O, O=C—O, C—O and O—C—O are located on the graphene surface. Stretching vibrations of —OH, C=O of carboxylic, O=C—O of carboxylate, C—O and C—O—C groups centered at 3500–2900, 1800, 1400, 1200 and 1100 cm^{-1}, respectively. Also, the peak at 1600 cm^{-1} is attributed to the vibrations of the adsorbed water molecules and also the vibrations of graphene skeletal. Comparison of FT-IR spectra of graphene and MnO_2/G nanocomposite are shown in Fig. 8.

The XRD patterns of Mn/G nanocomposite are shown in Fig. 9a. Graphene has a dominant peak centered at $2\theta = 26.5^\circ$

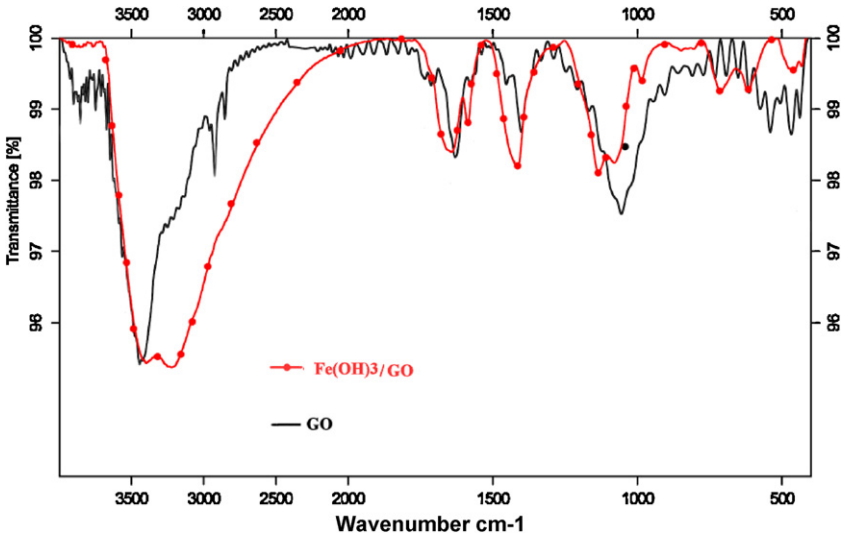

Fig. 11. FT-IR spectra of graphene oxide and $Fe(OH)_3$/GO. (For interpretation of the references to color in this figure legend, the reader is referred to the web version of this article.)

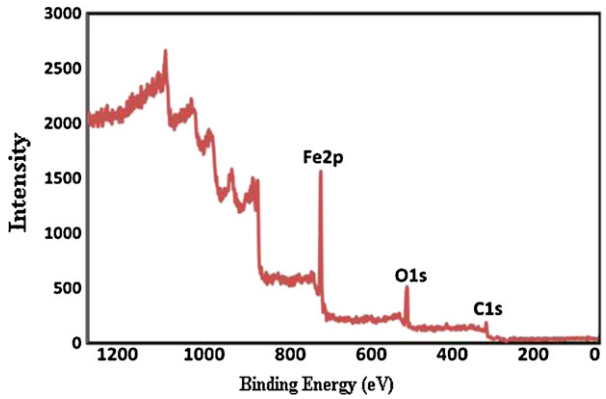

Fig. 12. XPS global survey of the surface of $Fe(OH)_3$/GO nanocomposite.

corresponding to an interlayer spacing of 3.356–3.361 Å. After reaction in presence of MnO_4^-, the interlayer spacing of the composite reached to 4.858 Å. It is slightly larger than *d*-spacing of graphene. The increased *d*-spacing for Mn/G composite can be ascribed to the presence of amounts of MnO_2 groups on the graphene surface.

As can be seen from the SEM image (Fig. 10a), the graphene nanosheets are well decorated with MnO_2 nanoparticles. Almost

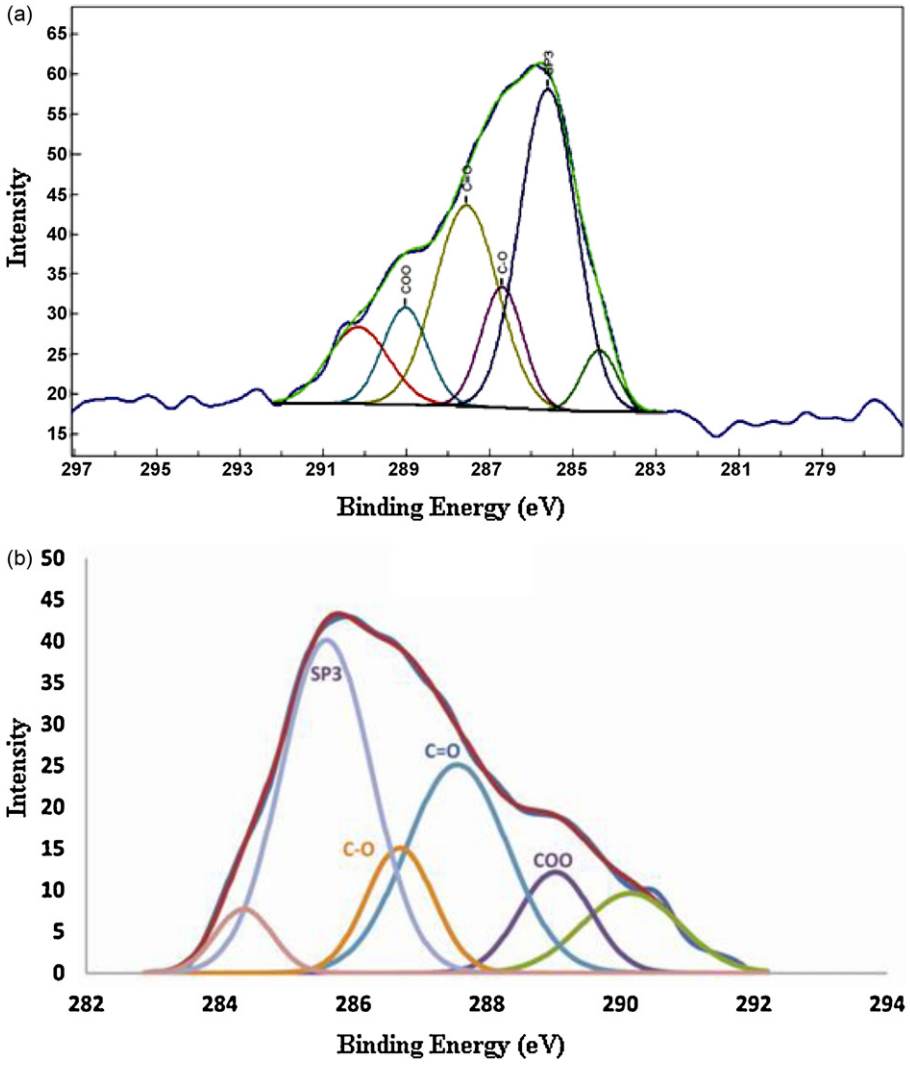

Fig. 13. XPS (a) general and (b) curve fit of C 1s.

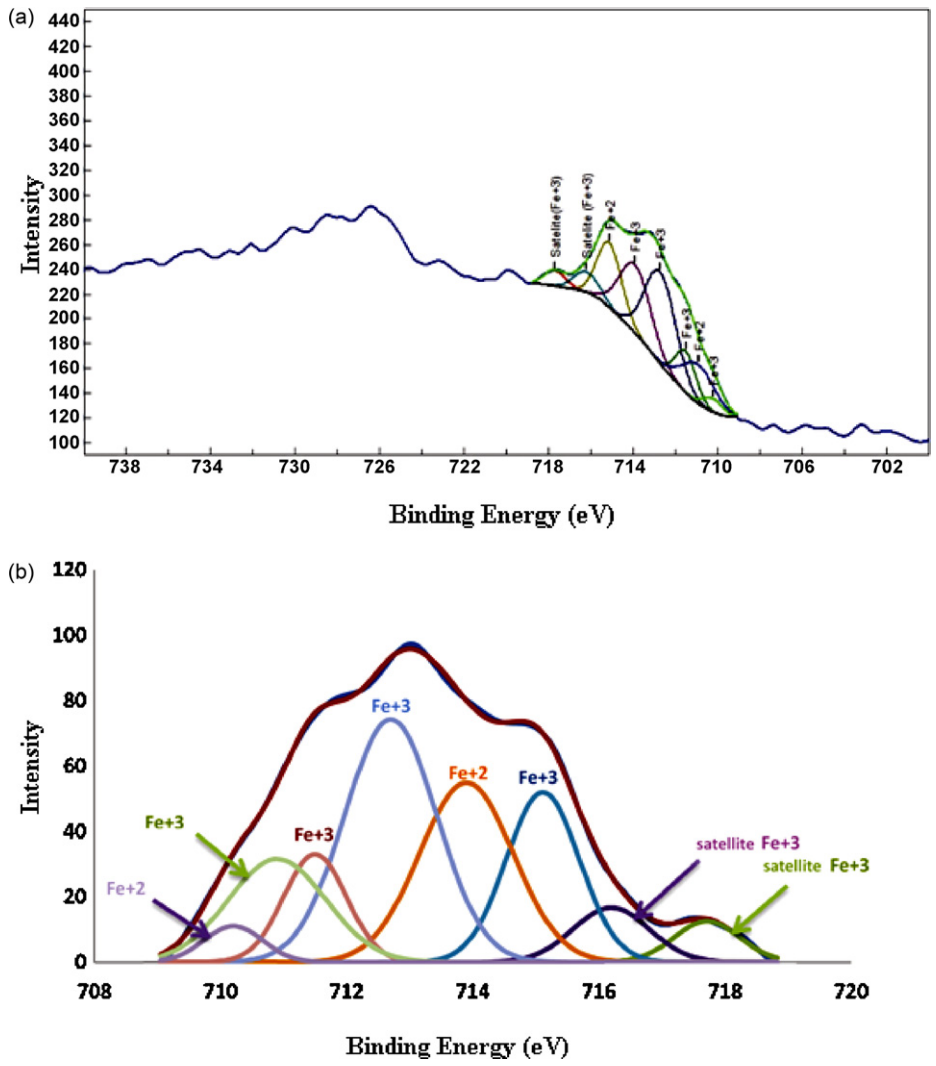

Fig. 14. XPS (a) general and (b) curve fit of 2p 3/2 spectroscopic state of iron.

no free MnO_2 nanoparticles are detected outside of the graphene sheets, indicating the perfect combination between nanoparticles and graphene nanosheets. The higher magnification SEM images which clearly demonstrate the dense and homogeneous distribution of nanoparticles on the surface of graphene sheets. The EDS pattern of MnO_2/G shown in Fig. 10b confirms that the existence of the elements of Mn besides C and O, demonstrating the successful deposition of MnO_2. The mass ratios of G:MnO_2 was 7.87.

3.4. Characterization of $Fe(OH)_3$/GO nanocomposite

Graphite oxide contained a variety of functional groups including —COOH, —OH and epoxy. Then iron ions coordinated to the surface of graphite oxide, transformed into ferric hydroxide nanoparticles through addition of ammonium hydroxide. The functionalization of graphene oxide with ferric hydroxide was further confirmed by the FT-IR (Fig. 11). Some bands that related with the oxygen-containing functional groups changed in the FT-IR spectra of this composite. Furthermore, weak peak at 607 cm^{-1} is observed suggesting the presence of Fe—O.

The XRD patterns of the synthesized composite with $Fe(OH)_3$ are shown in Fig. 9b. The diffraction peak of graphite oxide appeared at $2\theta = 12.2^\circ$ which originated from the diffraction on its (0 0 2) layer planes with the basal spacing of 0.722 nm. When graphene oxide was converted to $Fe(OH)_3$/GO composite, that were diminished which clearly signified the removal of oxy-functional groups. The XRD pattern, described the formation of ferric hydroxide on to the surface of graphene nanosheet as the peaks centered at $2\theta = 26^\circ$ and basal spacing of 0.803 nm. The broad nature and low relative intensity of the peak suggest amorphous nature of $Fe(OH)_3$ phase in composite and the small size of this particles (Li, Wang, Liu, Liu, & Yang, 2011).

The surfaces of $Fe(OH)_3$/GO nanocomposite was analyzed by XPS. The global survey by XPS is presented in Fig. 12. In this composite, the following peaks appeared: (i) iron (2p signal from 705 to 730 eV); (ii) oxygen (1s signal from 528 to 535 eV); (iii) carbon (1s signal from 282 to 290 eV). Figs. 13 and 14 present the C 1s and 2p3/2 spectrum of iron, respectively. The characteristics (position, FWHM and proportion) of the XPS C 1s and Fe 3p peak are reported in Tables 2 and 3, respectively.

The element mapping images of SEM clearly illustrated the deposition of nanoparticles in size of 24.5 nm onto the surfaces of graphene sheets (Fig. 15a and b). The added FeOH

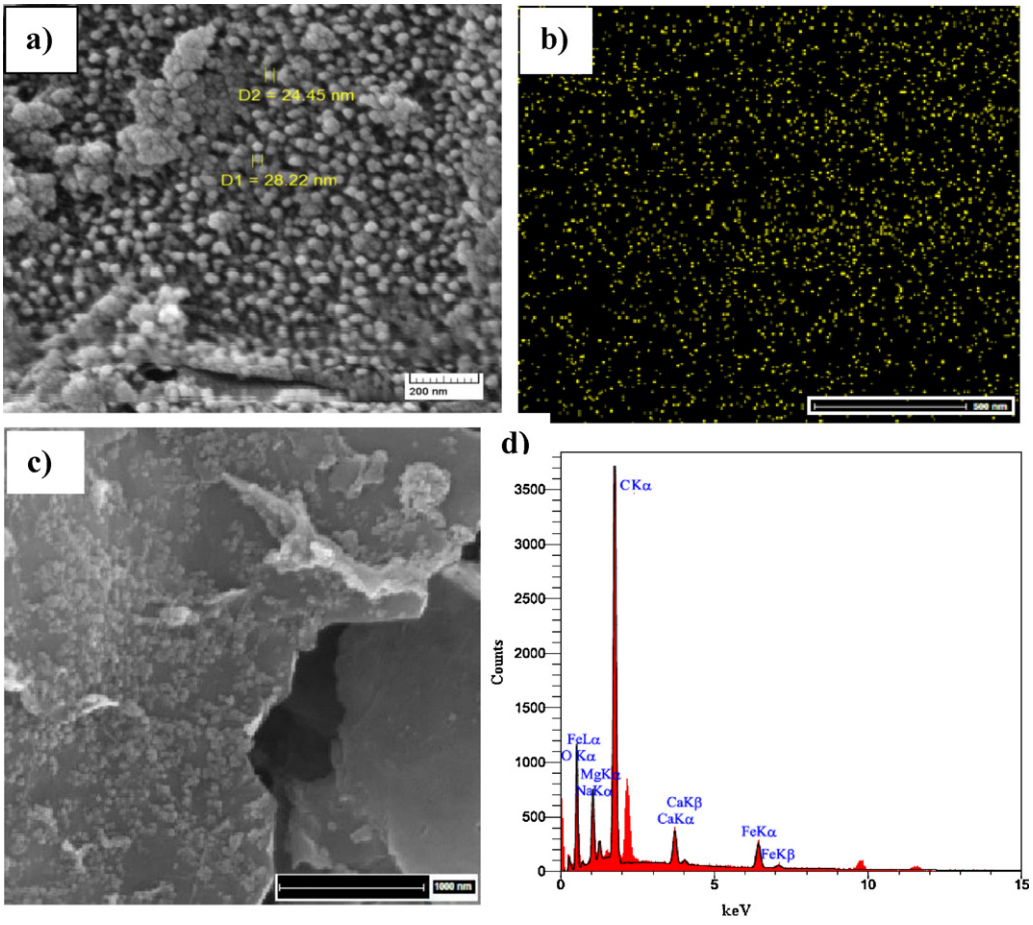

Fig. 15. SEM micrographs and corresponding EDS patterns of $Fe(OH)_3$/GO nanocomposite.

nanoparticles to the surface of graphene oxide appeared as bright dots that uniformly spread on the surface of the Fe/GO nanocomposite (Fig. 15b). It could be attributed to that most of the impregnated iron was in a coordination form with oxygen groups on the graphene oxide rather than in the free ferric hydroxide form. Images of this composite show formation of ferric oxide particles embedded within graphene oxide layers (Fig. 15c). The component of prepared composites was confirmed by energy dispersive X-ray spectroscopy (EDS) (Fig. 15d). The mass ratios of GO:Fe was 2.46.

Table 2
Position, FWHM, peak area and proportion of the XPS C 1s.

	BE (eV)	Peak area (cts)	FWHM (eV)	Proportion (%)
COO	289.03	16.6	1.28	9.3
C=O	287.56	47.8	1.79	26.9
C—O	286.70	19.2	1.19	10.8
SP^3	285.60	68.4	1.60	38.4

Table 3
Position, FWHM, peak area and proportion of the XPS Fe 3p.

	BE (eV)	Peak area (cts)	FWHM (eV)	Proportion (%)
Satellite Fe^{+3}	717.71	1.22	1.22	3.4
Satellite Fe^{+3}	716.19	1.42	1.42	5.3
Fe^{2+}	715.11	75.6	1.37	16.1
Fe^{3+}	713.90	102.3	1.75	21.7
Fe^{3+}	712.70	136.0	1.72	28.9
Fe^{3+}	711.50	41.3	1.17	8.8
Fe^{2+}	710.90	61.4	1.83	13.0
Fe^{3+}	710.20	12.8	1.10	2.7

3.5. Characterization of Co/G nanocomposite

When a graphene oxide sheet solution is mixed with a $Co(NO_3)_2{\cdot}6H_2O$ solution, Co^{2+} is bonded through electrostatic attraction. Since graphene oxide is homogeneously dispersed and the Co^{2+} are excluded each other, all Co^{2+} ion are uniformly dispersed on the surface and interlayer of graphene oxide sheets. Then in chemical reduction step eliminated all bands attributed to oxygen-containing groups by $NaBH_4$ and thus the graphene oxide was effectively transformed into graphene in the syntheses. Under ultrasonification condition, the interlayer spacing gradually increases and Co^{2+} ions could inter-laminate pore easily into the graphene enlarged layer.

The XRD pattern of Co/G nanocomposite is shown in Fig. 9c. The peak at $2\theta = 12.2^\circ$ corresponding to graphene oxide cannot be detected in this composite, which indicates that graphene oxide has been completely converted to graphene (peak at 25.1°). This peak related to a poorly crystallized compound originating from the small particle size and an approximately amorphous nature of the powder. Also, the peak at $2\theta = 43^\circ$ corresponding to the (1 0 0) crystal plane of graphene weakened after the deposition of cobalt, indicating that the surfaces of graphene are fully covered by nanoparticles cobalt.

Fig. 16a and b shows the SEM images of this composite. It is clear that Co nanoparticles (18.78 nm) are homogeneously coated on the graphene sheets. The EDS pattern (Fig. 16c) confirms the

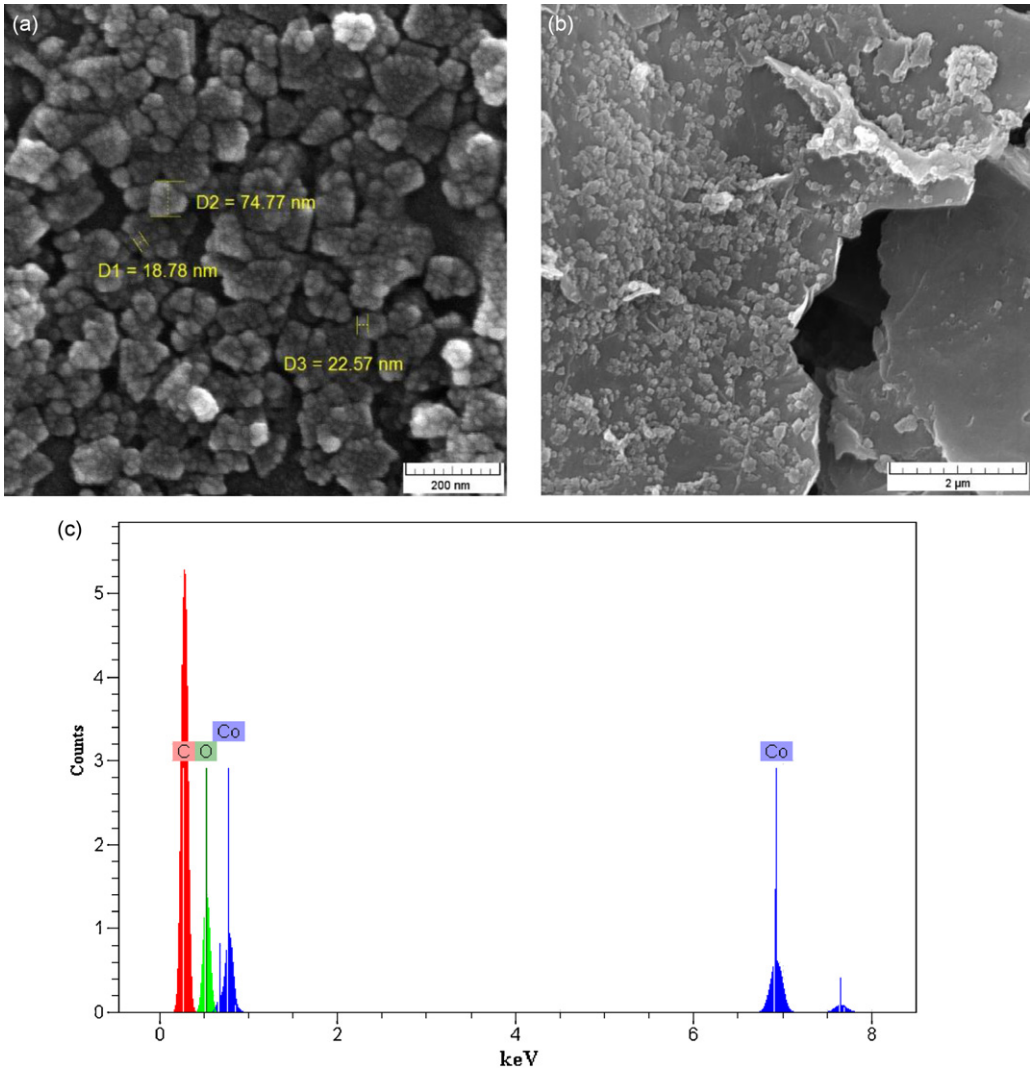

Fig. 16. (a, b) SEM micrographs and (c) corresponding EDS patterns of Co/G nanocomposite.

existence of the elements of Co, C and O, demonstrating the successful decoration of cobalt nanoparticles. The mass ratios of G:Co was 7.32.

4. Conclusions

In summary, graphene oxide and graphene nanosheets have been prepared in using a soft chemistry approach via Staudenmaier method. With the chemical procedure used, graphene oxide was prepared using concentrated sulfuric acid, nitric acid and potassium chlorate from raw graphite. The steps of oxidation, ultrasonic treatment and chemical reduction process yielded graphene nanosheets. The results from each step were investigated in details by FT-IR, Raman, XRD, SEM, EDS, AFM, and XPS. The analysis of structural changes from raw graphite to graphene oxide and graphene nanosheets in FT-IR, Raman spectra and XRD investigated. SEM observations confirmed the crystalline nature of graphene nanosheets and also demonstrated that graphene nanosheets naturally corrugated into ripples, like wavy silk.

Also, the present work showed immobilization of MnO_2, $Fe(OH)_3$ and cobalt nanoparticles on the graphene based nanosheets. All the results demonstrated that interaction between graphene oxide as matrix and metal nanoparticles were via hydroxyl, carbonyl and/or carboxylate groups. These nanoparticles were homogeneously distributed on the matrix of graphene sheets.

References

Berger, C., Song, Z. M., Li, T. B., Li, X. B., Ogbazghi, A. Y., Feng, R., et al. (2004). Ultrathin epitaxial graphite: Two-dimensional electron gas properties and a route toward graphene-based nanoelectronics. *Journal of Physical Chemistry B*, *108*, 19912–19916.

Berger, C., Song, Z. M., Li, X. B., Wu, X. S., Brown, N., Nand, C., et al. (2006). Electronic confinement and co-herence in patterned epitaxial graphene. *Science*, *312*, 1191–1196.

Dikin, D. A., Stankovich, S., Zimney, E. J., Piner, R. D., Dommett, G. H. B., Evmenenko, G., et al. (2007). Preparation and characterization of graphene oxide paper. *Nature*, *448*, 457–4560.

Guo, J., Zhu, S., Chen, Z., Li, Y., Yu, Z., Liu, Q., et al. (2011). Sonochemical synthesis of TiO_2 nanoparticles on graphene for use as photocatalyst. *Ultrasonics Sonochemistry*, *18*, 1082–1090.

He, H., Klinowski, J., Foster, M. A., & Lerf, A. (1998). A new structural model for graphite oxide. *Chemical Physics Letters*, *287*, 53–56.

Hirata, M., Gotou, T., Horiuchi, S., Fujiwara, M., & Ohba, M. (2004). Thin-film particles of graphite oxide 1: High-yield synthesis and flexibility of the particles. *Carbon*, *42*, 2929–2937.

Hontoria-Lucas, C., López-Peinado, A., López-González, J., & Martin-Aranda, R. (1995). Study of oxygen-containing groups in a series of graphite oxides: Physical and chemical characterization. *Carbon*, *33*, 1585–1592.

Ji, Z., Shena, X., Song, Y., & Zhu, G. (2011). In situ synthesis of graphene/cobalt nanocomposites and their magnetic properties. *Materials Science and Engineering B*, *176*, 711–715.

Li, Z., Wang, J., Liu, S., Liu, X., & Yang, S. (2011). Synthesis of hydrothermally reduced graphene/MnO_2 composites and their electrochemical properties as supercapacitors. *Journal of Power Sources*, *196*, 8160–8165.

Metin, Ö., Kayhan, E., Özkar, S., & Schneider, J. J. (2012). Palladium nanoparticles supported on chemically derived graphene: An efficient and reusable catalyst for the dehydrogenation of ammonia borane. *International Journal of Hydrogen Energy*, *37*, 8161–8169.

Novoselov, K. S., Geim, A. K., Morozov, S. V., Jiang, D., Katsnelson, M. I., Grigorieva, I. V., et al. (2005). Two-dimensional gas of massless Dirac fermions in graphene. *Nature*, *438*, 197–200.

Novoselov, K. S., Geim, A. K., Morozov, S. V., Jiang, D., Zhang, Y., Dubonos, S. V., et al. (2004). Electric field effect in atomically thin carbon films. *Science*, *306*, 666–669.

Reina, A., Jia, X., Ho, J., Nezich, D., Son, H., Bulovic, V., et al. (2009). Large area few-layer graphene films on arbitrary substrates by chemical vapor deposition. *Nano Letters*, *9*, 30–35.

Siamaki, A. R., Khder, A. E. R. S., Abdelsayed, V., El-Shall, M. S., & Gupton, B. F. (2011). Microwave-assisted synthesis of palladium nanoparticles supported on graphene: A highly active and recyclable catalyst for carbon–carbon cross-coupling reactions. *Journal of Catalysis*, *279*, 1–11.

Singh, V. K., Patra, M. K., Manoth, M., Gowd, G. S., Vadera, S. R., & Kumar, N. (2009). In situ synthesis of graphene oxide and its composites with iron oxide. *New Carbon Materials*, *24*, 147–152.

Stankovich, S., Dikin, D. A., Dommett, G. H. B., Kohlhaas, K. M., Zimney, E. J., Stach, E. A., et al. (2006). Graphene-based composite materials. *Nature*, *442*, 282–286.

Staudenmaier, L. (1898). Verfahren zur darstellung der graphitsäure. *Berichte der Deutschen Chemischen Gesellschaft*, *31*, 1481–1487.

Subrahmanyam, K. S., Manna, A. K., Pati, S. K., & Rao, C. N. R. (2010). A study of graphene decorated with metal nanoparticles. *Chemical Physics Letters*, *497*, 70–75.

Truong-Huu, T., Chizari, K., Janowska, I., Moldovan, M. S., Ersen, O., Nguyen, L. D., et al. (2012). Few-layer graphene supporting palladium nanoparticles with a fully accessible effective surface for liquid-phase hydrogenation reaction. *Catalysis Today*, *189*, 77–82.

Wang, G., Yang, J., Park, J., Gou, X., Wang, B., Liu, H., et al. (2008). Facile synthesis and characterization of graphene nanosheets. *Journal of Physical Chemistry C*, *112*, 8192–8195.

Wang, H. W., Hu, Z. A., Chang, Y. Q., Chen, Y. L., Lei, Z. Q., Zhang, Z. Y., et al. (2010). Facile solvothermal synthesis of a graphene nanosheet–bismuth oxide composite and its electrochemical characteristics. *Electrochimica Acta*, *55*, 8974–8980.

Yan, J., Fan, Z., Wei, T., Qian, W., Zhang, M., & Wei, F. (2010). Fast and reversible surface redox reaction of graphene–MnO_2 composites as supercapacitor electrodes. *Carbon*, *48*, 3825–3833.

Zhang, k., Dwivedi, V., Chi, C., & Wu, J. (2010). Graphene oxide/ferric hydroxide composites for efficient arsenate removal from drinking water. *Journal of Hazardous Materials*, *182*, 162–168.

Zhang, Y., Small, J. P., Amori, M. E. S., & Kim, P. (2005). Electric field modulation of galvanomagnetic properties of mesoscopic graphite. *Physical Review Letters*, *94*, 176803.

Zhang, Y., Tan, Y.-W., Stormer, H. L., & Kim, P. (2005). Experimental observation of the quantum Hall effect and Berry's phase in graphene. *Nature*, *438*, 201–204.